

Effects of coupling to vibrational modes on the ac conductance of molecular junctions

A. Ueda,^{1,*} O. Entin-Wohlman,^{1,†} and A. Aharony^{1,†}

¹*Department of Physics, Ben Gurion University, Beer Sheva 84105, Israel*

We theoretically examine the effect of the coupling of the transport electrons to a vibrational mode of the molecule on the ac linear-response conductance of molecular junctions. Representing the molecule by a single electronic state, we find that at very low temperatures the frequency-dependent conductance is mainly enhanced (suppressed) by the electron-vibration interaction when the chemical potential is below (above) the energy of that state. The vertex corrections of the electron-vibration interaction induce an additional peak structure in the conductance, which can be observed by tuning the tunnel couplings with the leads.

PACS numbers: 71.38.-k, 73.63.Kv, 73.21.La

I. INTRODUCTION

The fabrication of junctions made of small molecules seems by now well established.^{1–12} The transport properties of such molecular junctions are largely determined by the interplay between the electrical and the vibrational degrees of freedom. These include the couplings of the bridge with the leads, as well as the resonance energies. Their effects on the dc conductance of such junctions have been examined in many works (see below). Here we study the ac conductance, concentrating on the modulation of the frequency dependence brought about by the coupling to the vibrational modes. Our calculation is confined to the linear-response regime, and is carried out to second order in the coupling with the vibrational modes.

The simplest model for describing this system assigns a single electronic level, ε_0 , to the molecule, which is connected via two leads to two electronic reservoirs. Those are kept at different chemical potentials. When electrons pass through the molecule, they are coupled to its vibrational modes. Since the molecule has a finite size, those modes have finite frequencies; in the simplest approach and at very low temperatures, they may be represented by a single vibrational frequency, ω_0 , treated within the Einstein model. Various approximate numerical and analytical schemes have been developed for treating this model. The dc current-voltage characteristics have been studied by the perturbation theory,^{13–19} the rate equations,²⁰ and Monte Carlo methods.²¹ Furthermore, the shot noise and the full counting statistics of the charge passing the junction have been studied by perturbation theory,^{22–26} rate equations,²⁷ and the polaron approximation.^{28,29}

In the linear-response regime, the Breit-Wigner resonance of the dc conductance (as a function of the equilibrium chemical potential μ , and at very low temperatures) is *narrowed down* by the electron-vibration (e-v) interaction, due to the renormalization of the tunnel coupling between the molecule and the leads (the Frank-Condon blockade).^{19,20} However, the e-v interaction *does not* yield side peaks in the conductance at energies corresponding to the molecule vibrational frequencies, as long as it is not large enough to induce polaronic phase transitions. For such peaks to arise (at zero temperature and at small values of the e-v coupling), the electron needs to lose an energy ω_0 (we use $\hbar = 1$) in order to excite a vibrational mode, and this is not possible in the linear-response regime. Such side peaks will appear (at zero temperature) in

the *nonlinear*-response regime, where the finite voltage, V , allows for the opening of inelastic channels when eV exceeds ω_0 .^{14,19} Side peaks can be induced by a finite temperature, but their height will be minute, reflecting the number of available vibrational modes.¹⁹

The ac conductance of molecular junctions, in particular the effects of the e-v interaction on its frequency dependence, has been studied to lesser extent. Recently, Kubala and Marquardt³⁰ wrote down expressions for the ac conductance of interacting electrons traversing molecular junctions, in the case where the dc voltage is finite, while the ac one is very small, including as an example the e-v interaction. Our expressions (which are derived by a different approach) agree with theirs in the zero-dc bias limit. In addition, we give details of an extra diagram [(d) in Fig. 1] which they chose to ignore (because it vanishes in the dc limit), and present a detailed discussion of the dependence of the ac conductance on the various parameters.

As we show, the e-v interaction generates four contributions to the ac conductance. The first two are a Hartree and an exchange terms. In addition, the Kubo formula for the ac conductance also contains two vertex corrections. In the Keldysh formalism,^{31,32} the vertex corrections correspond to an expansion of the self energies in the time-dependent chemical potentials of the left and right reservoirs, $\delta\mu_L(t)$ and $\delta\mu_R(t)$, respectively. These corrections cause the ac conductance to diverge when the frequency ω of the applied ac voltage crosses ω_0 ; the imaginary part of the Green function of the vibrational mode is infinitesimally small to second-order in the e-v coupling. To avoid this divergence, a finite lifetime of the vibrational modes should be included. Two effects can be considered which contribute to this lifetime. One is the relaxation due to the coupling with bulk phonons in the substrate. We denote this relaxation rate by δ ; the other involves the electrical polarization, which results from the coupling of the vibrational mode with the transport electrons. The latter effect is dominant for floating molecules, air-bridged between the electrodes (in the absence of the substrate).¹³ We discuss this case in Sec. IV and in Appendix B.

The contributions of the vertex corrections to the ac conductance are proportional to the combination $\Gamma_L\delta\mu_L + \Gamma_R\delta\mu_R$, where $\Gamma_{L(R)}$ denotes the broadening of the energy level representing the molecule due to its coupling with the left (right) lead. Choosing a symmetric configuration, $\delta\mu_L(t) =$

$-\delta\mu_R(t)$ and $\Gamma_L = \Gamma_R$, causes these contributions to vanish. Therefore, in this symmetric case the ac conductance is affected by the e-v interaction only via the Hartree and the exchange (Fock) contributions. As we show, the former contribution is usually dominant, causing a relatively small increase (larger decrease) of the ac conductance when the average chemical potential in the leads, μ , is below (above) the electronic level ε_0 on the molecule. Similar to the dc conductance, this causes a narrowing of the ac conductance (plotted versus μ). Since the exchange contribution is even in $(\mu - \varepsilon_0)$, subtracting the conductances above and below ε_0 can yield information on the Hartree contribution. When the junction is not fully symmetric, the vertex corrections introduce an additional structure in the frequency dependence of the ac conductance, especially near $\omega = \pm\omega_0$. These corrections become maximal in the limit $\Gamma_L = \Gamma$ and $\Gamma_R = 0$.

The organization of the paper is as follows. We begin in Sec. II by describing our model and presenting the expression for the ac conductance of the system. The details of the derivation are relegated to Appendix A. Section III is devoted to the analysis of the results. In Sec. IV, we briefly discuss proposals for possible measurements and the effect of the electronic polarization on the conductance. The random-phase-approximation (RPA) treatment of the latter effect is outlined in Appendix B.

II. THE ac CONDUCTANCE

Our model system consists of two electronic reservoirs, connected together via a single electronic level ε_0 , which represents the molecule. The left and right reservoirs are kept at time-dependent chemical potentials, $\mu_L(t) = \mu + \delta\mu_L(t)$ and $\mu_R(t) = \mu + \delta\mu_R(t)$, which oscillate with frequency ω . When the electron is on the molecule, it is coupled to a local vibrational mode of frequency ω_0 . This simplified model is described by the Hamiltonian

$$\mathcal{H} = \mathcal{H}_{\text{lead}} + \mathcal{H}_{\text{mol}} + \mathcal{H}_{\text{tun}}. \quad (1)$$

It consists of the leads' Hamiltonian

$$\mathcal{H}_{\text{lead}} = \sum_k (\varepsilon_k - \mu_L) c_k^\dagger c_k + \sum_p (\varepsilon_p - \mu_R) c_p^\dagger c_p, \quad (2)$$

the Hamiltonian of the molecule

$$\mathcal{H}_{\text{mol}} = \varepsilon_0 c_0^\dagger c_0 + \omega_0 b^\dagger b + \gamma(b + b^\dagger) c_0^\dagger c_0, \quad (3)$$

and the tunneling Hamiltonian describing the coupling between the molecule and the leads

$$\mathcal{H}_{\text{tun}} = \sum_k (t_L c_k^\dagger c_0 + \text{h.c.}) + \sum_p (t_R c_p^\dagger c_0 + \text{h.c.}) \quad (4)$$

Here, $c_{k(p)}^\dagger$ and $c_{k(p)}$ denote the creation and annihilation operators of an electron of momentum $k(p)$ in the left (right) lead, respectively. The creation and annihilation operators on the level ε_0 are denoted by c_0^\dagger and c_0 , and $b^\dagger(b)$ creates (annihilates) a vibrational mode of frequency ω_0 . The coupling

of the transport electrons with the vibrational mode is scaled by γ . The broadening of the resonant level on the molecule, $\Gamma = \Gamma_L + \Gamma_R$, is given by $\Gamma_{L(R)} = 2\pi\nu|t_{L(R)}|^2$, with ν being the density of states of the electrons in the leads.

The current flowing into the molecule from the left reservoir may be expressed in terms of the Keldysh Green functions,^{31,32}

$$\begin{aligned} I_L(t) = & -2e\text{Re} \int dt' \sum_k |t_L|^2 [G_{00}^r(t, t') g_k^<(t', t) \\ & + G_{00}^<(t, t') g_k^a(t' - t) - g_k^r(t - t') G_{00}^<(t', t) \\ & - g_k^<(t, t') G_{00}^a(t', t)], \end{aligned} \quad (5)$$

with an analogous expression for the current coming from the right reservoir (with L replaced by R and k replaced by p). Here,

$$\begin{aligned} G_{00}^r(t, t') = & -i\theta(t - t') \langle \{c_0(t), c_0^\dagger(t')\} \rangle, \\ G_{00}^<(t, t') = & i \langle c_0(t') c_0^\dagger(t) \rangle, \end{aligned} \quad (6)$$

are the retarded and lesser Green functions on the molecule, where $\langle \dots \rangle$ denotes a quantum and statistical average over the states of the whole system. On the other hand, the retarded and lesser Green functions on the left (right) lead,

$$\begin{aligned} g_{k(p)}^r(t, t') = & -i\theta(t - t') \langle \{c_{k(p)}(t), c_{k(p)}^\dagger(t')\} \rangle_0, \\ g_{k(p)}^<(t, t') = & i \langle c_{k(p)}^\dagger(t') c_{k(p)}(t) \rangle_0. \end{aligned} \quad (7)$$

are given by the average $\langle \dots \rangle_0$ over the noninteracting leads alone.

Figure 1 depicts the diagrams of the linear-response ac conductance: (a) in the absence of the e-v interaction, (b) including the self energy from the Hartree term and (c) including the exchange term. Diagrams (d) and (e) are the vertex corrections of (b) and (c), respectively. The solid line indicates the Green function of the electron on the molecule whereas the dotted line denotes the Green function of the vibrational mode. The wavy line indicates the frequency of the ac field. The diagrams in Fig. 1 are also listed in Ref. 30. However, the diagram (d) was not calculated in that reference. Our expressions for the other diagrams agree with those of Ref. 30.

We expand Eq. (5) to first order in $\delta\mu_L(t)$ and $\delta\mu_R(t)$ as detailed in Appendix A. The linear-order currents $I_{L(R)}^1(\omega)$ are obtained by substituting the expansions (A10) and (A11) into Eqs. (A1) and (A2), and then substituting the latter expansions into Eq. (5). In our two-lead system, the linear-response ac conductance can be expressed as a matrix,

$$e \begin{bmatrix} I_L^1(\omega) \\ I_R^1(\omega) \end{bmatrix} = \begin{bmatrix} G_{LL}(\omega) & G_{LR}(\omega) \\ G_{RL}(\omega) & G_{RR}(\omega) \end{bmatrix} \begin{bmatrix} \delta\mu_L \\ \delta\mu_R \end{bmatrix}. \quad (8)$$

We show in Sec. III that when the molecule is coupled symmetrically to the leads, $\Gamma_L = \Gamma_R$, and the ac voltage is applied symmetrically as well, $\delta\mu_L(\omega) = -\delta\mu_R(\omega) = \delta\mu(\omega)/2$, the conductance pertaining to the net current is given by

$$G(\omega) = e \frac{I_L^1(\omega) - I_R^1(\omega)}{2\delta\mu(\omega)} = G_{LL}(\omega) - G_{RR}(\omega). \quad (9)$$

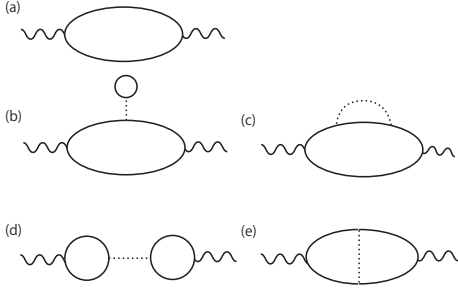


FIG. 1: The diagrams of the ac conductance: (a) without the e-v interaction, (b) the Hartree term, (c) the exchange term, (d) the vertex correction for the Hartree term and (e) the vertex correction for the exchange term. The solid line denotes the Green function of the electrons while the dotted line indicates the Green function of the vibrational mode. The wavy line indicates the frequency of the external ac field.

In this case, diagrams (d) and (e) (see Fig. 1) vanish since $\Delta_{2L} = \Delta_{2R} = 0$ [see Eqs. (A16); $\Delta_{2L(R)} = \Gamma_{L(R)}(\Gamma_L \delta\mu_L + \Gamma_R \delta\mu_R)$]. Consequently, the conductance given in Eq. (9) can be presented as a sum of three terms,

$$G(\omega) = G_{\text{nint}}(\omega) + G_{\text{H}}(\omega) + G_{\text{ex}}(\omega), \quad (10)$$

where

$$\begin{aligned} G_{\text{nint}}(\omega) &= e \frac{I_{L-\text{nint}}^1(\omega) - I_{R-\text{nint}}^1(\omega)}{2\delta\mu(\omega)}, \\ G_{\text{H}}(\omega) &= e \frac{I_{L-\text{H}}^1(\omega) - I_{R-\text{H}}^1(\omega)}{2\delta\mu(\omega)}, \\ G_{\text{ex}}(\omega) &= e \frac{I_{L-\text{ex}}^1(\omega) - I_{R-\text{ex}}^1(\omega)}{2\delta\mu(\omega)}, \end{aligned} \quad (11)$$

and the partial currents appearing in Eqs. (11) are given in Appendix A, see Eqs. (A15), (A19), and (A21). The conductance pertaining to the fully-symmetric junction, [see Eqs. (9) and (10)] is analyzed in the next section.

In the maximally asymmetric tunneling configuration, where $\Gamma_L = \Gamma$ and $\Gamma_R = 0$, the conductance of the junction is given by

$$G(\omega) = eI_L^1(\omega)/\delta\mu_L(\omega) = G_{LL}(\omega). \quad (12)$$

In this case there are contributions also from the vertex corrections, diagrams (d) and (e) of Fig. 1. We analyze the conductance of this configuration in Sec. III, expressing it in the form

$$\begin{aligned} G(\omega) &= G_{\text{nint}}(\omega) + G_{\text{H}}(\omega) \\ &\quad + G_{\text{ex}}(\omega) + G_{\text{verH}}(\omega) + G_{\text{verex}}(\omega). \end{aligned} \quad (13)$$

Here, each of the partial conductances is given by the respective partial current [see Eqs. (A15), (A19), (A21), (A22), and (A23)], divided by $\delta\mu_L(\omega)/e$.

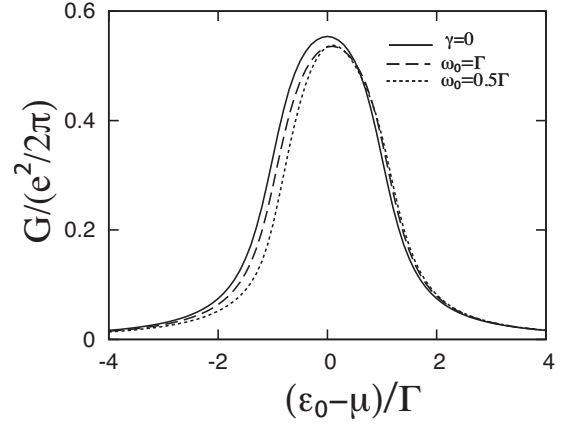


FIG. 2: The ac conductance of a fully-symmetric bridge, as a function of $\varepsilon_0 - \mu$ at $\omega = \Gamma$. The coupling strength of the e-v interaction is $\gamma = 0.3\Gamma$, and the frequency of the vibrational mode is $\omega_0 = \Gamma$ (dashed line) and $\omega_0 = 0.5\Gamma$ (dotted line). The solid line is the 'bare' conductance G_{nint} , obtained in the absence of the e-v interaction.

III. NUMERICAL RESULTS FOR THE ac CONDUCTANCE

As explained in Sec. I, one has to allow for a finite lifetime for the vibrational mode (even at lowest-order in the coupling γ), in order to avoid unphysical divergences. In this section we assume a constant relaxation rate (adopting the value $\delta = 0.1\Gamma$ for the numerical computations); possible contributions of the transport electrons to this rate are discussed in the next section. In the following we measure all energies in units of Γ , the broadening of the resonance molecular electronic level brought about by the coupling to the leads.

We begin with the case of a symmetrically-coupled junction, $\Gamma_L = \Gamma_R$. Figure 2 shows the conductance G , Eq. (9), as a function of $\varepsilon_0 - \mu$, for a fixed ac frequency $\omega = \Gamma$. The solid line indicates G_{nint} , the conductance in the absence of the e-v coupling. It is seen that the resonance peak does not reach unity as happens in the case of the dc conductance,^{14,19} due to the suppression by the ac field. When the e-v coupling is accounted for (the dashed and dotted lines in Fig. 2) this peak becomes somewhat narrower, which is more remarkable for smaller ω_0 . This behavior of the resonance peak is qualitatively similar to the dc case.¹⁹

Furthermore, the center of the resonance peak shifts to a higher energy as compared to the one in the absence of the e-v coupling. The narrowing and the shift may be understood by including the Hartree term self-consistently in the electron Green function [Eq. (A12)] employing the Dyson equation

$$\begin{aligned} G_{00}^r(\omega) &= G_{00}^{r(0)}(\omega) + G_{00}^{r(0)}(\omega)\Sigma_{\text{H}}^r(0)G_{00}^r(\omega), \\ &\cong 1/[\omega - \varepsilon_0 + i\Gamma/2 - \Sigma_{\text{H}}^r(0)]. \end{aligned} \quad (14)$$

As can be seen from Eq. (A20), $\Sigma_{\text{H}}^r(0)$ is negative, and consequently the localized level representing the molecule is shifted to a lower energy, implying a lower (higher) conductance for $\varepsilon_0 < \mu$ ($\varepsilon_0 > \mu$). Also the Hartree term renormalizes the energy scale, which contributes to the narrowing. This renormalization is due to the polaron binding energy. Notice that

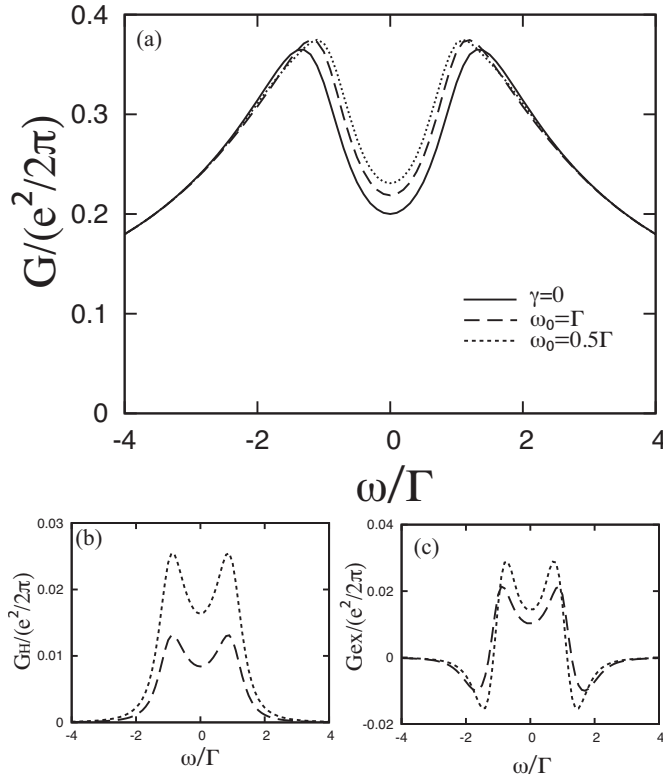


FIG. 3: (a) The ac conductance of the fully-symmetric bridge, as a function of the frequency of the bias voltage ω , at $\varepsilon_0 - \mu = \Gamma$ and $\gamma = 0.3\Gamma$. The frequency of the vibrational mode is $\omega_0 = \Gamma$ (dashed line) and $\omega_0 = 0.5\Gamma$ (dotted line). The solid line is the ‘bare’ conductance G_{nint} , in the absence of the e-v interaction. (b) The additional conductance due to the Hartree term of the e-v interaction. (c) The additional conductance due to the exchange term.

the energy scale is also renormalized by the exchange term, which oppositely tends to broaden the resonance peak. However, this effect is smaller than that of the Hartree one (as long as δ remains small). Since in the linear-response regime there is no real exchange of energy between the electrons and the vibrational mode, no additional peak structure appears in the conductance.

The full conductance G , Eq. (9), as a function of the ac frequency ω of the external bias when $\varepsilon_0 - \mu = \Gamma$, is depicted in Fig. 3 (a). The solid line indicates the conductance in the absence of the e-v coupling, G_{nint} . Two broad peaks appear around ω of order $\pm 1.5(\varepsilon_0 - \mu)$. The broken lines show G in the presence of the e-v interaction with $\omega_0 = \Gamma$ or $\omega_0 = 0.5\Gamma$. The e-v interaction increases the conductance in the region between the original peaks, shifting these peaks to lower $|\omega|$, while decreasing the conductance slightly outside this region, where the e-v effect decays very quickly. Figures 3 (b) and (c) portray the contributions to the conductance due to the e-v interaction coming from the Hartree and the exchange terms [diagrams (b) and (c) in Fig. 1], G_{H} and G_{ex} respectively, for the same parameters. Similar results arise for all positive $\varepsilon_0 - \mu$. Both G_{H} and G_{ex} show two sharp peaks around $\omega \sim \pm(\varepsilon_0 - \mu)$ (causing the increase in G and the shift in

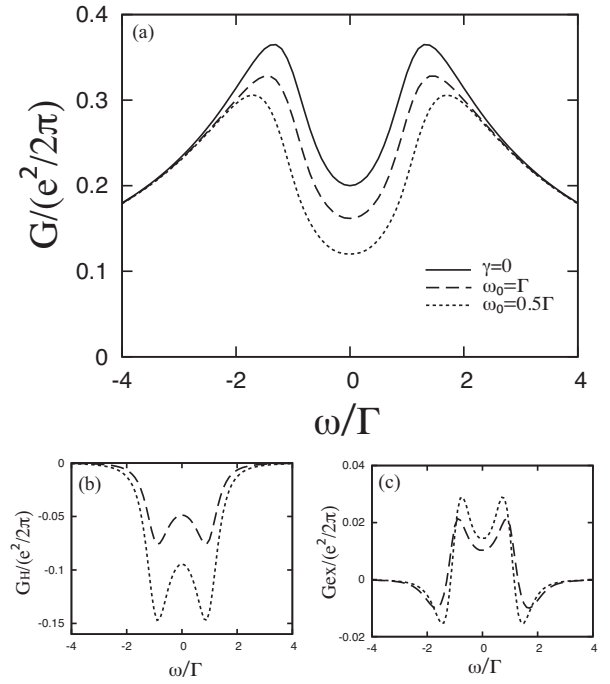


FIG. 4: The same as Fig. 3, but with $\varepsilon_0 - \mu = -\Gamma$.

its peaks), and both decay rather fast outside this region. In addition, G_{ex} also exhibits two negative minima, leading to small ‘shoulders’ in the total G which are not much visible in Fig. 3 (a). The exchange term virtually shifts the polaron level on the molecule, yielding an enhancement in the conductance. The amount of increase is more dominant for lower ω_0 . The situation reverses for $\varepsilon_0 < \mu$, as seen in Fig. 4. Here, G_{nint} remains as before, but the ac conductance is suppressed by the e-v interaction. The additional conductance is dominated by G_{H} . The Hartree term of the e-v interaction renormalizes the energy level in the molecule to lower values, resulting in the suppression of G , while G_{ex} coincides with the case for $\varepsilon_0 - \mu = \Gamma$. The amount of decrease is larger for lower ω_0 . Figures 3 and 4 show that the sign of change in the conductance depends on the sign of the Hartree contribution, G_{H} .

Next, we consider the conductance Eq. (13) of an asymmetrically-coupled bridge for which $\Gamma_{\text{L}} = \Gamma$ and $\Gamma_{\text{R}} = 0$. In this case the vertex corrections are required as explained in Sec. II. Figure 5 shows the conductance as a function of the bias frequency ω when $\varepsilon_0 - \mu = \Gamma$ (panel a) and $\varepsilon_0 - \mu = -\Gamma$ (panel b). Similar to the conductance of a symmetrically-coupled junction ($\Gamma_{\text{L}} = \Gamma_{\text{R}}$), the ac conductance is enhanced or suppressed as compared to the noninteracting case, depending on whether $\varepsilon_0 > \mu$ or $\varepsilon_0 < \mu$. The contributions to the conductance arising from the vertex corrections to the Hartree and the exchange diagrams, G_{verH} and G_{verex} [see Eq. (13)] are shown in panels (c) and (d) respectively. The vertex corrections coincide for $\varepsilon_0 - \mu = \pm\Gamma$. Interestingly, the plot (c) exhibits sharp peaks at $\omega = \pm\omega_0$ due to the singularities of the Green function of the vibrational mode, which are smeared by its lifetime. These also appear as anomalous peaks in the to-

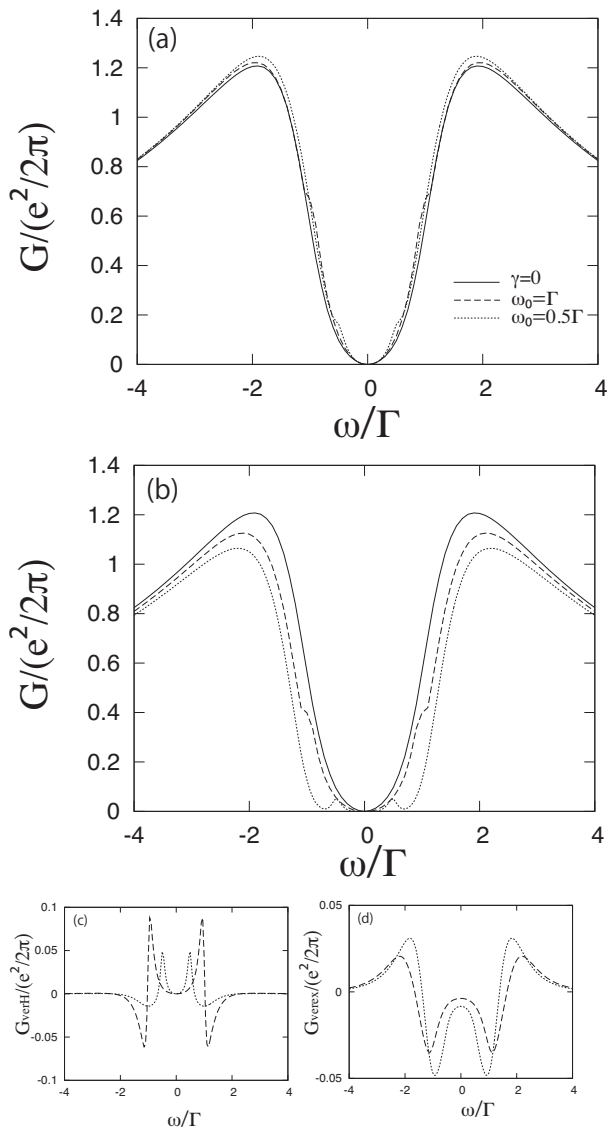


FIG. 5: The ac conductance of an asymmetric junction, as a function of ω at (a) $\varepsilon_0 - \mu = \Gamma$ and (b) $\varepsilon_0 - \mu = -\Gamma$ when $\Gamma_L = \Gamma$. The energy of the vibrational mode is $\omega_0 = \Gamma$ (dashed line) or $\omega_0 = 0.5\Gamma$ (dotted line). The solid line is the ‘bare’ conductance G_{inint} , in the absence of the e-v interaction. The additional conductances resulting from the vertex corrections of the Hartree and exchange terms are shown in panels (c) and (d).

tal conductance. This is due to the charge fluctuation caused by the ac field, which leads to a fluctuation of the vibrational mode. This effect becomes blurred when the relaxation rate δ is large. Note that the contributions of the vertex correction of the exchange diagram, G_{verex} , cancels some amount of G_{ex} , therefore the enhancement of the conductance is not large for $\varepsilon_0 > \mu$.

IV. DISCUSSION AND SUMMARY

Figures 3 and 4 show that within our perturbative expansion the effect of the e-v interaction on the ac conductance is relatively small and the results do not differ qualitatively from the expectation without this interaction. One way to focus on the e-v effect is to compare the conductances at $\varepsilon_0 - \mu = \Gamma$ and $\varepsilon_0 - \mu = -\Gamma$. As mentioned in Sec. III, all the contributions to the conductance except the one coming from the Hartree term, G_{H} , are the same for $\varepsilon_0 - \mu = \Gamma$ and $\varepsilon_0 - \mu = -\Gamma$. Therefore, one can measure the difference $G_{\text{H}} - G'_{\text{H}}$ by subtracting the total conductance G' for $\varepsilon_0 - \mu = -\Gamma$ from G for $\varepsilon_0 - \mu = \Gamma$. Another effect which can be observable involves the sharp peaks due to the vertex correction of the Hartree term. This effect is only visible when the combination $\Gamma_L \delta \mu_L + \Gamma_R \delta \mu_R$ is large and the relaxation time δ is small compared to Γ . Tuning the tunneling energies $\Gamma_{L(R)}$ can help to extract these effects from the data.

As stated, the vibrational lifetime for floating molecules (that are not placed on a substrate) may be dominated by the effect of the electronic polarization (i.e., the self energy of the vibration due to the coupling with the transport electrons), which also smears the singularities of the Green functions of the vibrational mode D^α (α takes the values r , a , or $<$) in Eqs. (A6) and (A7). In this case, at order γ^2 , D^α is replaced by Eqs. (B1) or (B2) in Appendix B, which include the RPA-type dressing by electrons shown as the thick dotted line in Fig. 6. Thus, all the dotted lines in Fig. 1 are replaced by the thicker dotted line. As discussed in Appendix B, this procedure generates an additional lifetime for the vibrational modes. For $\gamma^2/(\omega_0\Gamma) < 1/4$ we find that the effect of these RPA-type dressings on the conductance is similar to that of the effective ‘ad hoc’ relaxation rate δ , as reported previously.³³ For larger e-v coupling γ , the energy shift of the electronic level representing the molecule ε_0 [which corresponds to $\Sigma_{\text{H}}^r(0)$ in Eq. (A18)] is no longer monotonic as a function of ε_0 . This may imply the breakdown of the perturbation expansion.

As mentioned in the introduction, and seen in Eqs. (A22) and (A23), the vertex contributions [diagrams (d) and (e) of Fig. 1] appear only for asymmetrically-coupled bridges. It is diagram (d) of Fig. 1 that is most sensitive to the vibrational mode lifetime, since its contribution is explicitly proportional to the vibrational Green function (the dotted line in the center of the diagram). Our results for the symmetric case, based on diagrams (a)-(c), are indeed not very sensitive to the vibrational mode lifetime. The RPA treatment of the electronic polarization for the case in which the molecule is coupled *asymmetrically* to the leads requires several additional terms. In addition to diagrams (d) and (e) of Fig. 1, in the asymmetric case we also need to add diagrams (f) and (g) of Fig. 6, which represent the vertex corrections to diagrams (b) and (c) of Fig. 1. However, these new contributions involve higher orders of the e-v coupling γ , and thus go beyond the scope of the present paper.

In summary, we have studied the effect of the e-v interaction on the ac linear conductance of molecular junctions, employing a simple model. The e-v interaction enhances or suppresses the conductance, depending on whether the energy

level of the orbital in the molecule is higher or lower than the chemical potential. When the tunnel coupling is asymmetric as defined in Sec. II above, an additional anomalous structure appears at $\omega = \pm\omega_0$ due to fluctuations caused by the ac field.

Acknowledgments

The authors thank Y. Utsumi for useful discussions. This work was partially supported by the German Federal Ministry of Education and Research (BMBF) within the framework of

the German-Israeli project cooperation (DIP), and by the US-Israel Binational Science Foundation (BSF).

Appendix A: Details of the current derivation

As mentioned, our calculation is carried out to second-order in the coupling of the transport electrons to the vibrations, γ . Thus the Dyson equations for the Green functions on the molecule are³⁴

$$G_{00}^{r[a]}(t, t') = G_{00}^{r[a](0)}(t - t') + \int dt_1 G_{00}^{r[a](0)}(t - t_1) \Sigma_{\text{H}}^{r[a]}(t_1, t_1) G_{00}^{r[a](0)}(t_1 - t') + \int dt_1 \int dt_2 G_{00}^{r[a](0)}(t - t_1) \Sigma_{\text{ex}}^{r[a]}(t_1, t_2) G_{00}^{r[a](0)}(t_2 - t'), \quad (\text{A1})$$

and

$$G_{00}^{<}(t, t') = G_{00}^{<(0)}(t, t') + \int dt_1 G_{00}^{r(0)}(t - t_1) \Sigma_{\text{H}}^r(t_1, t_1) G_{00}^{<(0)}(t_1, t') + \int dt_1 G_{00}^{<(0)}(t, t_1) \Sigma_{\text{H}}^a(t_1, t_1) G_{00}^{a(0)}(t_1 - t') + \int dt_1 \int dt_2 G_{00}^{r(0)}(t - t_1) \Sigma_{\text{ex}}^r(t_1, t_2) G_{00}^{<(0)}(t_2, t') + \int dt_1 \int dt_2 G_{00}^{<(0)}(t, t_1) \Sigma_{\text{ex}}^a(t_1, t_2) G_{00}^{a(0)}(t_2 - t') + \int dt_1 \int dt_2 G_{00}^{r(0)}(t - t_1) \Sigma_{\text{ex}}^{<}(t_1, t_2) G_{00}^{a(0)}(t_2 - t'). \quad (\text{A2})$$

Here, $\Sigma_{\text{H}}^r(t, t)$ represents the self energy due to the Hartree term [diagram (b) in Fig. 1],

$$\Sigma_{\text{H}}^r(t, t) = -i\gamma^2 \int dt' G_{00}^{<(0)}(t', t') D^r(t - t'), \quad (\text{A3})$$

and $\Sigma_{\text{H}}^a(t, t) = \Sigma_{\text{H}}^r(t, t)$. The contribution of the Fock term [diagram (c) in Fig. 1], $\Sigma_{\text{ex}}^\alpha(t, t')$, where α takes the values r , a or $<$, is

$$\Sigma_{\text{ex}}^r(t, t') = i\gamma^2 [G_{00}^{<(0)}(t, t') D^r(t - t') + G_{00}^{a(0)}(t - t') D^<(t - t') \pm G_{00}^{a(0)}(t - t') D^r(t - t')], \quad (\text{A4})$$

and

$$\Sigma_{\text{ex}}^{<}(t, t') = i\gamma^2 G_{00}^{<(0)}(t, t') D^<(t - t'). \quad (\text{A5})$$

Here, $G_{00}^{\alpha(0)}(t - t')$ are the Green functions in the absence of the e-v interaction.

The Green functions pertaining to the vibrational mode are given by

$$D^r(t - t') = -i\theta(t - t') \langle [b(t) + b^\dagger(t)], [b(t') + b^\dagger(t')] \rangle \quad (\text{A6})$$

and

$$D^<(t - t') = -i \langle [b(t') + b^\dagger(t')], [b(t) + b^\dagger(t)] \rangle. \quad (\text{A7})$$

To second-order in γ , these are required only to order γ^0 . However, as explained in Sec. I, there is a need to assign a finite lifetime to the vibrations. Here we take the relaxation rate (i.e., the inverse lifetime) to be a constant, δ , arising from a possible coupling to a substrate. A different scenario is considered in Appendix B. Thus, the Fourier transforms of the vibrational Green functions (at zero temperature) are

$$D^r(\omega) = \frac{1}{\omega - \omega_0 + i\delta} - \frac{1}{\omega + \omega_0 + i\delta}, \quad D^a(\omega) = [D^r(\omega)]^*, \quad (\text{A8})$$

and

$$D^<(\omega) = \frac{1}{\omega + \omega_0 + i\delta} - \frac{1}{\omega + \omega_0 - i\delta}. \quad (\text{A9})$$

Note that all the Green functions except $G_{00}^{<(0)}(t, t')$ and $g_{00}^{<(0)}(t, t')$ depend only on the time difference $t - t'$.

We expand the Green functions pertaining to the electrons to the first order in the chemical potentials $\delta\mu_{\text{L}}(\omega)$ and $\delta\mu_{\text{R}}(\omega)$,

$$g_{k(p)}^{<}(t, t') \approx if[\xi_{k(p)}]e^{-i\xi_{k(p)}(t-t')} \exp[i \int_{t'}^t dt_1 \delta\mu_{L(R)}(t)] = if[\xi_{k(p)}]e^{-i\xi_{k(p)}(t-t')} \left\{1 - \int \frac{d\omega}{2\pi\omega} [e^{-i\omega t} - e^{-i\omega t'}] \delta\mu_{L(R)}(\omega)\right\}, \quad (\text{A10})$$

and

$$G_{00}^{<(0)}(t, t') \approx \int \frac{d\omega}{2\pi} e^{-i\omega(t-t')} if(\omega) \Gamma G_{00}^{r(0)}(\omega) G_{00}^{a(0)}(\omega) + \int d\omega \int d\omega' \frac{i}{(2\pi)^2 \omega} [f(\omega + \omega') - f(\omega')] e^{-i(\omega + \omega')t} e^{i\omega't'} G_{00}^{r(0)}(\omega + \omega') G_{00}^{a(0)}(\omega') (\Gamma_L \delta\mu_L + \Gamma_R \delta\mu_R), \quad (\text{A11})$$

where $\xi_k = \varepsilon_k - \mu$ and $f(\omega) = 1/[\exp(\omega/k_B T) + 1]$ is the Fermi distribution function of the leads. The Fourier transform of the retarded Green function of the molecule is

$$G_{00}^{r(0)}(\omega) = \frac{1}{\omega - \varepsilon_0 + i\Gamma/2}, \quad (\text{A12})$$

and the advanced Green function is $G_{00}^{a(0)}(\omega) = [G_{00}^{r(0)}(\omega)]^*$.

Once the current emerging from the left lead, Eq. (5), is expanded to linear order in $\delta\mu_L$ and $\delta\mu_R$, it is convenient to

divide its Fourier transform into five parts,

$$I_L^1(\omega) = I_{L-\text{nint}}^1(\omega) + I_{L-\text{H}}^1(\omega) + I_{L-\text{ex}}^1(\omega) + I_{L-\text{verH}}^1(\omega) + I_{L-\text{verex}}^1(\omega). \quad (\text{A13})$$

The first term on the right-hand side of Eq. (A13) is the current in the absence of the e-v interaction,

$$I_{L-\text{nint}}^1(\omega) = \frac{e}{2\pi\omega} \int d\omega' [f(\omega + \omega') - f(\omega')] \text{Re}\{-i\Delta_{1L}[G_{00}^{r(0)}(\omega + \omega') - G_{00}^{a(0)}(\omega')] + \Delta_{2L}G_{00}^{r(0)}(\omega + \omega')G_{00}^{a(0)}(\omega')\}. \quad (\text{A14})$$

Carrying out the frequency integration, we find

$$I_{L-\text{nint}}^1(\tilde{\omega}) = \frac{e\Gamma}{2\pi} \text{Re}\left\{[(i\tilde{\omega} - 1)\tilde{\Delta}_{1L} + \tilde{\Delta}_{2L}] \frac{1}{2\tilde{\omega}(i + \tilde{\omega})} \{-2i \arctan[2(\tilde{\omega} - \tilde{\varepsilon}_0)] - 2i \arctan[2(\tilde{\omega} + \tilde{\varepsilon}_0)] + \log[1 + 4(\tilde{\omega} - \tilde{\varepsilon}_0)^2] + \log[1 + 4(\tilde{\omega} + \tilde{\varepsilon}_0)^2] - 2 \log[1 + 4\tilde{\varepsilon}_0^2]\}\right\}. \quad (\text{A15})$$

We have introduced in Eq. (A14) the notations

$$\begin{aligned} \Delta_{1L} &= \Gamma_L \delta\mu_L, \\ \Delta_{2L} &= \Gamma_L(\Gamma_L \delta\mu_L + \Gamma_R \delta\mu_R). \end{aligned} \quad (\text{A16})$$

In Eq. (A15) and below, we denote by tilde all variables divided by Γ (assigning for them the same notations as before).

The second term on the right-hand side of Eq. (A13) is the contribution of the self energy resulting from the Hartree term Σ_H [diagram (b) in Fig. 1],

$$\begin{aligned} I_{L-\text{H}}^1(\omega) &= \frac{e}{2\pi\omega} \int d\omega' [f(\omega + \omega') - f(\omega')] \\ &\times \text{Re}\left\{[-i\Delta_{1L}\{[G_{00}^{r(0)}(\omega + \omega')]^2 - [G_{00}^{a(0)}(\omega')]^2\} + \Delta_{2L}\{[G_{00}^{r(0)}(\omega + \omega')]^2 G_{00}^{a(0)}(\omega') + G_{00}^{r(0)}(\omega + \omega')[G_{00}^{a(0)}(\omega')]^2\}\right\} \Sigma_H^r(0). \end{aligned} \quad (\text{A17})$$

Here, $\Sigma_H^r(0)$ is

$$\Sigma_H^r(0) = \frac{\gamma^2}{2\pi} \int_{-\infty}^0 d\omega \Gamma G_{00}^{r(0)}(\omega) G_{00}^{a(0)}(\omega) D^r(0). \quad (\text{A18})$$

Performing the integration in Eq. (A17) yields

$$I_{L-\text{H}}^1(\tilde{\omega}) = \frac{e\Gamma}{2\pi} \text{Re}\left\{\frac{32\tilde{\varepsilon}_0[(i\tilde{\omega} - 1)\tilde{\Delta}_{1L} + \tilde{\Delta}_{2L}]}{(1 + 4\tilde{\varepsilon}_0^2)[4\tilde{\varepsilon}_0^2 - (i + 2\tilde{\omega})^2]}\right\} \tilde{\Sigma}_H^r(0), \quad (\text{A19})$$

with

$$\tilde{\Sigma}_H^r(0) = -\frac{\tilde{\gamma}^2}{\pi} [\pi - 2 \arctan(2\tilde{\varepsilon}_0)] \frac{\tilde{\omega}_0}{\tilde{\omega}_0^2 + \tilde{\delta}^2}. \quad (\text{A20})$$

The contribution of the exchange terms [diagram (c) in Fig. 1] to the current is

$$I_{L-\text{ex}}^1(\omega) = \frac{e}{2\pi\omega} \int d\omega' [f(\omega + \omega') - f(\omega')] \text{Re}(-i\Delta_{1L}[G_{00}^{r(0)}(\omega + \omega')\Sigma_{\text{ex}}^r(\omega + \omega')G_{00}^{r(0)}(\omega + \omega') - G_{00}^{a(0)}(\omega')\Sigma_{\text{ex}}^a(\omega')G_{00}^{a(0)}(\omega')] + \Delta_{2L}\{[G_{00}^{r(0)}(\omega + \omega')]^2\Sigma_{\text{ex}}^r(\omega + \omega')G_{00}^{a(0)}(\omega') + G_{00}^{r(0)}(\omega + \omega')[G_{00}^{a(0)}(\omega')]^2\Sigma_{\text{ex}}^a(\omega')\}. \quad (\text{A21})$$

Finally, the last two terms on the right-hand side of Eq. (A13) are

$$I_{L-\text{verH}}^1(\omega) = \frac{e\gamma^2}{(2\pi)^2\omega} \int d\omega' \int d\omega'' \text{Re}\{i\Delta_{2L}[f(\omega + \omega') - f(\omega'')G_{00}^{r(0)}(\omega + \omega')G_{00}^{a(0)}(\omega')D^r(\omega) \times [f(\omega + \omega'') - f(\omega'')]G_{00}^{r(0)}(\omega + \omega'')G_{00}^{a(0)}(\omega'')\} = \frac{e\tilde{\gamma}^2\Gamma}{(2\pi)^2} \text{Re}\left(\frac{\tilde{\Delta}_{2L}}{2\tilde{\omega}(i + \tilde{\omega})^2} \{-2i \arctan[2(\tilde{\omega} - \tilde{\varepsilon}_0)] - 2i \arctan[2(\tilde{\omega} + \tilde{\varepsilon}_0)] + \log[1 + 4(\tilde{\omega} - \tilde{\varepsilon}_0)^2] + \log[1 + 4(\tilde{\omega} + \tilde{\varepsilon}_0)^2] - 2\log[1 + 4\tilde{\varepsilon}_0^2]\}^2 \frac{\tilde{\omega}_0}{(\tilde{\omega} + i\tilde{\delta})^2 - \tilde{\omega}_0^2}\right), \quad (\text{A22})$$

and

$$I_{L-\text{verex}}^1(\omega) = \frac{e\gamma^2}{(2\pi)^2\omega} \int d\omega' \int d\omega'' \text{Re}\{i\Delta_{2L}[-f(\omega + \omega')D^a(\omega' - \omega'') + f(\omega')D^r(\omega' - \omega'')] + D^<(\omega' - \omega'')][f(\omega + \omega'') - f(\omega'')]G_{00}^{r(0)}(\omega + \omega'')G_{00}^{a(0)}(\omega')G_{00}^{r(0)}(\omega + \omega'')G_{00}^{a(0)}(\omega'')\}. \quad (\text{A23})$$

We evaluate the integrals appearing in the expressions for $I_{L-\text{ex}}^1$ and $I_{L-\text{verex}}^1$ [Eqs. (A21) and (A23)] numerically as functions of $\tilde{\omega}$, $\tilde{\omega}_0$, and $\tilde{\varepsilon}_0$. The linear expansion of the current emerging from the right lead, I_R^1 , is calculated in the same way.

Appendix B: Green function of the vibrational mode including self energy corrections due to the transport electrons

Here we solve the Green function of the vibrational mode taking into account self energy corrections coming from the coupling with the transport electrons. We derive the electronic polarization induced by those electrons employing the random-phase-approximation (RPA).

The relevant diagrams are depicted in Fig. 6, leading to

$$D^{r[a]}(t, t') = D^{r[a](0)}(t - t') + \int dt_1 \int dt_2 D^{r[a](0)}(t - t_1)\Pi^{r[a]}(t_1, t_2)D^{r[a]}(t_2, t'), \quad (\text{B1})$$

and

$$D^<(t, t') = \int dt_1 \int dt_2 D^r(t, t_1)\Pi^<(t_1, t_2)D^a(t_2, t'). \quad (\text{B2})$$

Here, D^α [see Eqs. (A6) and (A7)] and $D^{\alpha(0)}$ are the Green function pertaining to the vibrational mode in the presence and absence of the coupling to the transport electrons, respectively; Π^α is the polarization,

$$\Pi^r(t, t') = -i\gamma^2[G_{00}^{<(0)}(t, t')G_{00}^{a(0)}(t' - t) + G_{00}^{r(0)}(t - t')G_{00}^{<(0)}(t', t)], \quad (\text{B3})$$

and

$$\Pi^<(t, t') = -i\gamma^2G_{00}^{<(0)}(t, t')G_{00}^{>(0)}(t', t). \quad (\text{B4})$$

The expressions for the polarization Π^α contain $G^{<(0)}$, which depends on the chemical potentials in the reservoirs. Expanding to linear order in $\delta\mu_{L(R)}$, yields diagrams (f) and (g) in Fig. 6. This order of the expansion turns out to be proportional to $\Gamma_L\delta\mu_L + \Gamma_R\delta\mu_R$, and therefore diagrams (f) and (g) of Fig. 6 do not contribute to the conductance of a fully-symmetric junction [Eq. (9)]. In any event, these diagrams involve higher orders in γ , and therefore we discard them hereafter.

Confining ourselves for simplicity to the case of a fully-symmetric junction [see Eq. (9)], it is sufficient to keep only the zeroth order for $G^{<(0)}$, which yields

$$D^{r[a]}(\tilde{\omega}) = \frac{1}{\Gamma} \frac{2\tilde{\omega}_0}{\tilde{\omega}^2 - \tilde{\omega}_0^2 - 2\tilde{\omega}_0\Pi^{r[a]}(\tilde{\omega})/\Gamma} \quad (\text{B5})$$

and

$$D^<(\tilde{\omega}) = D^r(\tilde{\omega})\Pi^<(\tilde{\omega})D^a(\tilde{\omega}), \quad (\text{B6})$$

where

$$\Pi^r(0) = -\frac{2\tilde{\gamma}^2\Gamma}{\pi(1 + 4\tilde{\varepsilon}_0^2)} \quad (\text{B7})$$

when $\tilde{\omega} = 0$. When $\tilde{\omega} \neq 0$ we have

$$\begin{aligned} \Pi^r(\tilde{\omega}) = & -i \frac{\tilde{\gamma}^2 \Gamma}{2\pi} \left[\frac{1}{2i + 2\tilde{\omega}} \{2i \arctan[2(\tilde{\omega} - \tilde{\varepsilon}_0)] + 2i \arctan[2(\tilde{\omega} + \tilde{\varepsilon}_0)]\} \right. \\ & + 2 \ln[1 + 4\tilde{\varepsilon}_0^2] - \ln[1 + 4(\tilde{\omega} - \tilde{\varepsilon}_0)^2] - \ln[1 + 4(\tilde{\omega} + \tilde{\varepsilon}_0)^2] \} \\ & \left. - \frac{1}{2\tilde{\omega}} (2i \arctan[2(\tilde{\omega} - \tilde{\varepsilon}_0)] + 2i \arctan[2(\tilde{\omega} + \varepsilon_0)] - \ln[1 + 4(\tilde{\omega} - \tilde{\varepsilon}_0)^2] - \ln[1 + 4(\tilde{\omega} + \tilde{\varepsilon}_0)^2] + 2 \ln[1 + 4\tilde{\varepsilon}_0^2]) \right], \quad (\text{B8}) \end{aligned}$$

and

$$\begin{aligned} \Pi^<(\tilde{\omega}) = & i \frac{\tilde{\gamma}^2}{2\pi} \frac{\Gamma}{\tilde{\omega} + \tilde{\omega}^3} \{2\tilde{\omega} \arctan[2(\tilde{\omega} - \tilde{\varepsilon}_0)] + 2\tilde{\omega} \arctan[2(\tilde{\omega} + \tilde{\varepsilon}_0)] \\ & + \ln[1 + 4(\tilde{\omega} - \tilde{\varepsilon}_0)^2] + \ln[1 + 4(\tilde{\omega} + \tilde{\varepsilon}_0)^2] - 2 \ln[1 + 4\tilde{\varepsilon}_0^2]\} \theta(-\tilde{\omega}). \quad (\text{B9}) \end{aligned}$$

Clearly, $\text{Im}\Pi^r(\tilde{\omega})$ and $\Pi^<(\tilde{\omega})$ yield a finite lifetime for the vibrational mode.

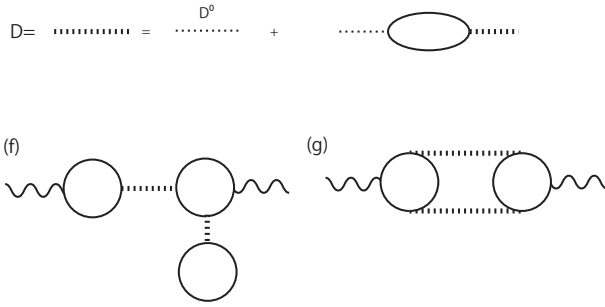


FIG. 6: Top: The thick dotted line denotes the Green function of the vibrational mode with the RPA term, see Eqs. (B1) and (B2). Bottom: The diagrams required when the RPA term is included besides the diagrams in Fig. 1 [with the replacement of the dotted line in Fig. 1 by the thick dotted line, as shown in the top part].

* Electronic address: akiko@bgu.ac.il

† Also at Tel Aviv University, Tel Aviv 69978, Israel

¹ M. A. Reed, C. Zhou, C. J. Muller, T. P. Burgin, and J. M. Tour, *Science* **278**, 252 (1997); J. Chen, M. A. Reed, A. M. Rawlett, and J. M. Tour, *ibid.* **286**, 1550 (1999).

² J. Reichert, R. Ochs, D. Beckmann, H. B. Weber, M. Mayor, and H. v. Lohneysen, *Phys. Rev. Lett.* **88**, 176804 (2002).

³ N. B. Zhitenev, H. Meng, and Z. Bao, *Phys. Rev. Lett.* **88**, 226801 (2002).

⁴ S. Kubatkin, A. Danilov, M. Hjort, J. Cornil, J. Bredas, N. Stuhr-Hansen, P. Hedegard, and T. Bjornholm, *Nature (London)* **425**, 698 (2003).

⁵ J. G. Kushmerick, J. Lazorek, C. H. Patterson, R. Shashidhar, D. S. Seferos, and G. C. Bazan, *Nano Lett.* **4**, 639 (2004).

⁶ X. H. Qiu, G. V. Nazin, and W. Ho, *Phys. Rev. Lett.* **92**, 206102 (2004).

⁷ H. Park, J. Park, A. K. L. Lim, E. H. Anderson, A. P. Alivisatos, and P. L. McEuen, *Nature (London)* **407**, 57 (2000); A. N. Pa-

supathy, J. Park, C. Chang, A. V. Soldatov, S. Lebedkin, R. C. Bialczak, J. E. Grose, L. A. K. Donev, J. P. Sethna, D. C. Ralph, and P. L. McEuen, *Nano Lett.* **5**, 203 (2005).

⁸ B. J. LeRoy, S. G. Lemay, J. Kong, and C. Dekker, *Nature (London)* **432**, 371 (2004).

⁹ R. H. M. Smit, Y. Noat, C. Untiedt, N. D. Lang, M. C. van Hemert, and J. M. van Ruitenbeek, *Nature (London)* **419**, 906 (2002); D. Djukic, K. S. Thygesen, C. Untiedt, R. H. M. Smit, K. W. Jacobsen, and J. M. van Ruitenbeek, *Phys. Rev. B* **71**, 161402 (2005); W. H. A. Thijssen, D. Djukic, A. F. Otte, R. H. Bremmer, and J. M. van Ruitenbeek, *Phys. Rev. Lett.* **97**, 226806 (2006).

¹⁰ S. Sapmaz, P. Jarillo-Herrero, Ya. M. Blanter, C. Dekker, and H. S. J. van der Zant, *Phys. Rev. Lett.* **96**, 026801 (2006).

¹¹ O. Tal, M. Krieger, B. Leerink, and J. M. van Ruitenbeek, *Phys. Rev. Lett.* **100**, 196804 (2008); M. Kiguchi, O. Tal, S. Wohlthat, F. Pauly, M. Krieger, D. Djukic, J. C. Cuevas, and J. M. van Ruitenbeek, *Phys. Rev. Lett.* **101**, 046801 (2008).

¹² R. Leturcq, C. Stampfer, K. Interbitzin, L. Durrer, C. Heirold, E.

- Mariani, M. G. Schultz, F. von Oppen, and K. Ensslin, *Nature Physics* **5**, 327 (2009).
- ¹³ M. Galperin, M. A. Ratner, and A. Nitzan, *Nano Lett.* **4**, 1605 (2004).
- ¹⁴ A. Mitra, I. Aleiner, and A. J. Millis, *Phys. Rev. B* **69**, 245302 (2004).
- ¹⁵ D. A. Ryndyk and J. Keller, *Phys. Rev. B* **71**, 073305 (2005).
- ¹⁶ O. Hod, R. Baer, and E. Rabani, *Phys. Rev. Lett.* **97**, 266803 (2006); *J. Phys: Condens. Matter*, **20**, 383201 (2008).
- ¹⁷ R. Egger and A. O. Gogolin, *Phys. Rev. B* **77**, 113405 (2008).
- ¹⁸ R-P. Riwar and T. L. Schmidt, *Phys. Rev. B* **80**, 125109 (2009).
- ¹⁹ O. Entin-Wohlman, Y. Imry, and A. Aharony, *Phys. Rev. B* **80**, 035417 (2009); O. Entin-Wohlman, Y. Imry, and A. Aharony, *Phys. Rev. B* **81**, 113408 (2010).
- ²⁰ J. Koch and F. von Oppen, *Phys. Rev. Lett.* **94**, 206804 (2005); J. Koch, M. Semmelhack, F. von Oppen, and A. Nitzan, *Phys. Rev. B* **73**, 155306 (2006).
- ²¹ L. Mühlbacher and E. Rabani, *Phys. Rev. Lett.* **100**, 176403 (2008).
- ²² M. Galperin, A. Nitzan, and M. A. Ratner, *Phys. Rev. B* **74**, 075326 (2006).
- ²³ T. L. Schmidt and A. Komnik, *Phys. Rev. B* **80**, 041307(R) (2009).
- ²⁴ R. Avriller and A. Levy Yeyati, *Phys. Rev. B* **80**, 041309(R) (2009).
- ²⁵ F. Haupt, T. Novotny, and W. Belzig, *Phys. Rev. Lett.* **103**, 136601 (2009); *Phys. Rev. B* **82**, 165441 (2010).
- ²⁶ D. F. Urban, R. Avriller, and A. Levy Yeyati, *Phys. Rev. B* **82**, 121414 (2010).
- ²⁷ R. Avriller, arXiv:1007.4450.
- ²⁸ J.-X. Zhu and A. V. Balatsky, *Phys. Rev. B* **67**, 165326 (2003).
- ²⁹ S. Maier, T. L. Schmidt, and A. Komnik, arXiv:1010.2918.
- ³⁰ B. Kubala and F. Marquardt, *Phys. Rev. B* **81**, 115319 (2010).
- ³¹ L. V. Keldysh, *Zh. Eksp. Teor. Fiz.* **47**, 1515 (1964) [*Sov. Phys. JETP* **20**,1018 (1965)].
- ³² H. J. W. Haug and A-P. Jauho, *Quantum Kinetics in Transport and Optics of Semiconductors* (Springer Verlag 2008).
- ³³ A. Ueda, O. Entin-Wohlman and A. Aharony, *Nanoscale Res. Lett.* (in press).
- ³⁴ G. D. Mahan, *Many-Particle Physics* (Plenum Press, New York, 1990).